Climate Feedbacks in Response to Changes in Obliquity

DAMIANOS F. MANTSIS AND AMY C. CLEMENT

Rosenstiel School of Marine and Atmospheric Science, University of Miami, Miami, Florida

ANTHONY J. BROCCOLI AND MICHAEL P. ERB

Department of Environmental Sciences, Rutgers, The State University of New Jersey, New Brunswick, New Jersey

(Manuscript received 9 August 2010, in final form 19 December 2010)

ABSTRACT

The feedbacks involved in the response of climate to a reduction of Earth's obliquity are investigated in the GFDL Climate Model version 2.1 (CM2.1). A reduction in obliquity increases the meridional gradient of the annual mean insolation, causing a strengthening of the atmospheric and ocean circulation that transports more heat poleward. The heat transport does not balance the direct obliquity forcing completely, and additional local radiative fluxes are required to explain the change in the equilibrium energy budget. The surface temperature generally increases at low latitudes and decreases at high latitudes following the change in the insolation. However, in some areas, the sign of the temperature change is opposite of the forcing, indicating the strong influence of feedbacks. These feedbacks are also responsible for a decrease in the global mean temperature despite that the change in the global mean insolation is close to zero. The processes responsible for these changes are increases in the ice fraction at high latitudes and the global cloud fraction—both of which reduce the absorbed solar radiation. A reduction in the global greenhouse trapping, due to changes in the distribution of the water vapor content of the atmosphere as well as a change in the lapse rate, has an additional cooling effect. Among these feedbacks, clouds and the lapse rate have the larger contribution, with water vapor and surface albedo having a smaller effect. The implications of the findings presented here for interpretation of obliquity cycles in the paleoclimate record are discussed.

1. Introduction

It is well known that after the mid-Pleistocene transition, about 0.8 Ma ago (where 1 Ma = 10^6 yr), the evolution of ice ages was dominated by 100-kyr (where 1 kyr = 1000 yr) cycles. However, during the late Pliocene and early Pleistocene [~(3.0–0.8) Ma], climate variability was dominated by obliquity-induced 41-kyr cycles (Raymo and Nisancioglu 2003). Obliquity is an astronomical parameter that represents earth's axial tilt, and fluctuates between values of 22° and 24.5° with a period of 41kyr. It affects Earth's climate by controlling the top-of-atmosphere (TOA) incoming solar radiation contrast between low and high latitudes, which drives the atmospheric general circulation and the associated meridional heat and moisture fluxes (Trenberth and Caron 2001). A lower axial tilt strengthens the annual mean meridional insolation gradient without affecting the global mean insolation (Lee and Poulsen 2005). The strong obliquity signal of Antarctica deuterium-excess records of the last 150 kyr confirms that an increased meridional insolation gradient, due to a reduction in Earth's axial tilt, strengthens the heat and moisture transport in the Southern Hemisphere (Vimeux et al. 1999).

North Atlantic alkenone-based sea surface temperature (SST) proxies (Lawrence et al. 2010) show that North Atlantic SSTs varied on the obliquity frequency during the late Pliocene and early Pleistocene, with temperatures being 2°–4°C lower when Earth's axial tilt and high-latitude insolation were reduced. Such cold surface (SFC) conditions in the North Atlantic favored North Atlantic deepwater formation, as suggested by deepwater temperature proxies based on Mg/Ca ratios from benthic foraminifera (Sosdian and Rosenthal 2009) and ostracodes (Dwyer et al. 1995). During the same period, global ice volume was also increased when Earth's axial tilt was lower, as suggested by the benthic δ^{18}O record (Raymo and Nisancioglu 2003). Changes in ice volume

Corresponding author address: Damianos F. Mantsis, RSMAS, University of Miami, Miami, FL 33149.
E-mail: dmantsis@rsmas.miami.edu

DOI: 10.1175/2010JCLI3986.1

are also supported by records of ostracode Mg/Ca data, which suggest that sea level was reduced by roughly 60–70 m when earth's axial tilt was lower (Dwyer et al. 1995).

During the same period, the tropical east Pacific was also 1°–2°C cooler when Earth's axial tilt was reduced, despite the increased insolation associated with it, as suggested by proxy records based on alkenone productivity (Lawrence et al. 2006; Liu and Herbert 2004). Using the same method, Cleaveland and Herbert (2007) show that the western tropical Pacific, eastern tropical Atlantic, Arabian Sea, and South China Sea SSTs were in phase with those in the east Pacific during the Pleistocene (last 2 Ma). Also, Medina-Elizalde and Lea (2005), and de Garidel-Thoron et al. (2005) confirmed, using SST records based on Mg/Ca ratios from foraminifera shells, that the west Pacific SSTs were in phase with those in the east Pacific. These studies imply that all the tropical oceans were cold when local TOA insolation increased. Such tropical SST variability cannot be directly forced by obliquity-induced insolation changes, and other mechanisms must be invoked to explain these results.

Phillips and Held (1994) showed that the tropics warm and the high latitudes cool when the obliquity is reduced, but their results were based on experiments with an atmospheric model coupled to a slab ocean model that does not include variations in ocean heat transport and used prescribed clouds. A more recent study by Lee and Poulsen (2005) showed using the Fast Ocean Atmosphere Model (FOAM) that the climate response to a reduction in obliquity is a slight global surface cooling (S.-Y. Lee 2009, personal communication). However, their findings also show that the SSTs warm throughout the tropical band between 30°S and 30°N, in contrast with all available proxy records. That study focused on the response of the tropical Pacific and did not address the atmospheric general circulation response and the associated heat transports, or the modulation of the orbital forcing by climate feedbacks.

The response of the coupled atmosphere–ocean system to an idealized change in obliquity is examined in this paper. For our purpose we use the Geophysical Fluid Dynamics Laboratory Climate Model version 2.1 (GFDL CM2.1) described, together with the experimental design, in section 2. Section 3 documents the temperature response. The atmospheric and ocean circulation response and the associated heat transport are addressed in section 4. In section 5 we decompose the global temperature response in terms of a local radiative balance and feedbacks [cloud, water vapor (WV), lapse rate, (LR) and ice]. A comparison of the model results with the available proxy record is presented in section 6, and the last section summarizes the conclusions and addresses the discussion.

2. Model description and experimental design

For this study we use the CM2.1 coupled atmosphere–ocean general circulation model developed at the National Oceanic and Atmospheric Administration's GFDL. As documented in detail by Delworth et al. (2006), CM2.1 is constructed from component models of the atmosphere (GFDL Global Atmospheric Model Development Team 2004; Lin 2004), land [based on the model of Milly and Shmakin (2002)], ocean (Gnanadesikan et al. 2006), and sea ice (Winton 2000). As implemented in CM2.1, the horizontal resolution of the atmosphere and land models is 2° latitude × 2.5° longitude, and the atmospheric model has 24 levels in the vertical. The resolution of the ocean component is 1° in latitude and longitude, with the meridional resolution equatorward of 30° latitude becoming progressively finer, such that it is $\frac{1}{3}$° at the equator. There are 50 vertical levels in the ocean, with 22 levels of 10-m thickness each in the top 220 m. The ocean component uses a true freshwater-flux boundary condition when precipitation and runoff enter the ocean. This contrasts with earlier ocean models employing the so-called rigid lid approximation, which requires the use of a virtual salt flux. The sea ice component of CM2.1 is a dynamical model with 3 vertical layers (1 snow and 2 ice) and 5 ice-thickness categories. The components of CM2.1 are coupled without using flux adjustments. The realistic simulation of the modern climate by CM2.1 makes it a good candidate for addressing the question regarding the response of climate to orbital forcing, despite some biases that are described in detail by Delworth et al. (2006) and Wittenberg et al. (2006).

The experiment consists of two simulations, designed to isolate the effect of variations in obliquity on climate. For this we will compare two model runs with obliquity values of 22.079° and 24.480° but holding other parameters [i.e., solar irradiance, greenhouse gas (GHG) concentrations, and surface boundary conditions] to the same values as those used in preindustrial (i.e., 1860) simulations with CM2.1 (Delworth et al. 2006). These obliquity values represent the extremes of obliquity variations during the last 600 kyr of the Quaternary (Berger and Loutre 1991). The chosen range of obliquity values is very representative of the range of obliquity variations during the last full glacial–interglacial cycle (22.235°–24.437°) and the past 5 Ma (22.079°–24.538°). Other orbital parameters, such as the eccentricity and the precession, were also held constant, with the eccentricity at 0.0172 and the longitude of the perihelion at 101.37°.

Each of these simulations is initialized from year 1000 of a preindustrial run of CM2.1, with the altered orbital parameters imposed instantaneously. From there each of these simulations is run for 600 yr, which should be

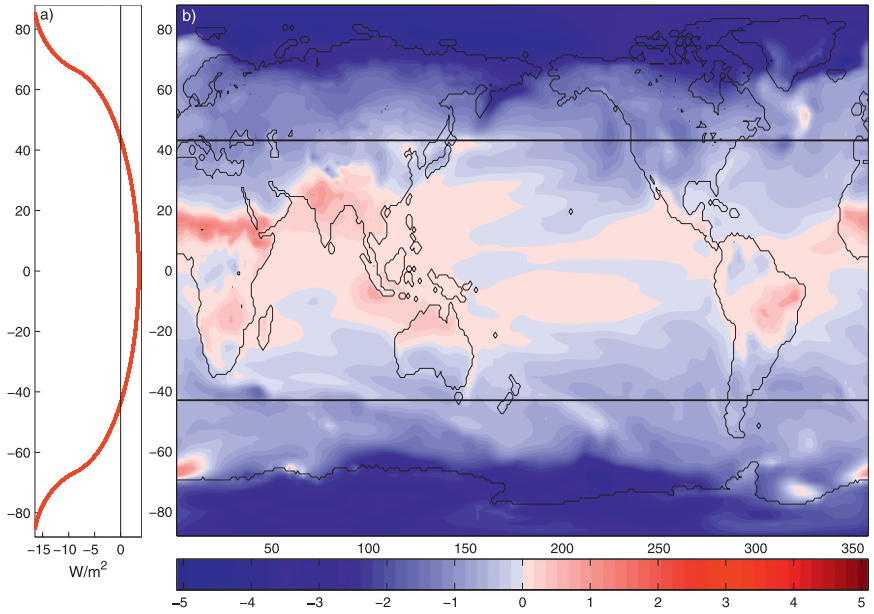

FIG. 1. Annual mean changes (low − high obliquity) of (a) SW incoming solar radiation at the TOA (W m^{-2}) and (b) surface temperature (°C). Black lines represent the latitude where the insolation change is 0.

sufficient for the surface and upper ocean to approach equilibrium (Hewitt and Mitchell 1998). However, it should be noted that the deep ocean still exhibits a small long-term temperature trend at the end of the 600-yr run that also has a small effect on the surface heat fluxes.

This study uses averages of the last 100 yr of each simulation and focuses on annual mean conditions. The following analysis concentrates on comparing atmospheric and oceanic diagnostics between the high- and low-obliquity simulation.

3. Temperature response

The effects of a change in Earth's obliquity (axial tilt) can be physically interpreted as a redistribution of the insolation by changing its meridional gradient, but at the same time keeping the total solar radiation incident upon the earth the same. On an annual mean basis, a reduction in the obliquity from 24.480° to 22.079° slightly increases the insolation at the equator by 3.5 W m^{-2} (0.8% increase); however, it causes a much larger reduction at the poles by 16 W m^{-2} (9.3% reduction) (Fig. 1a). The orbital forcing also exhibits substantial seasonal variation that reduces the seasonal contrast at each latitude, because of a reduction of the summer hemisphere insolation and a smaller increase of the winter hemisphere insolation. Here we focus on annual mean conditions, since that is how the temperature proxies are interpreted.

As the annual mean meridional gradient of the insolation intensifies, the meridional surface temperature gradient becomes stronger (Fig. 1b), with a warming in the tropics (maximum tropical warming is 0.8°C over the ocean and 1.5°C over the continents) and a cooling at high latitudes (maximum high-latitude cooling is 5.1°C). However, despite the positive forcing, the SSTs decrease in the midlatitudes, the subtropics, and parts of the tropics, implying that the forcing is overwhelmed by feedbacks. This is more evident on the eastern side of all basins, leading to a strengthening of the zonal SST gradient in the subtropics. The physical processes associated with this will be discussed in the next sections.

The changes in the zonal mean tropospheric temperature also consist of a weak increase in the tropics, and a cooling everywhere else (Fig. 2), with the zonal asymmetries seen in the surface temperature disappearing from the surface. A larger temperature increase in the upper troposphere, compared to the lower troposphere, results in a reduction of the vertical lapse rate in the tropics. At higher latitudes the lapse rate also decreases, but it is due to a larger temperature decrease in the lower troposphere than in the upper troposphere.

The local changes of the surface temperature, mentioned above, sum to a global mean surface cooling response (−0.55°C) for the low obliquity compared to the high-obliquity climate, despite that the incoming solar radiation does not change in the global mean sense. Lee and Poulsen (2005) showed in a similar experiment that

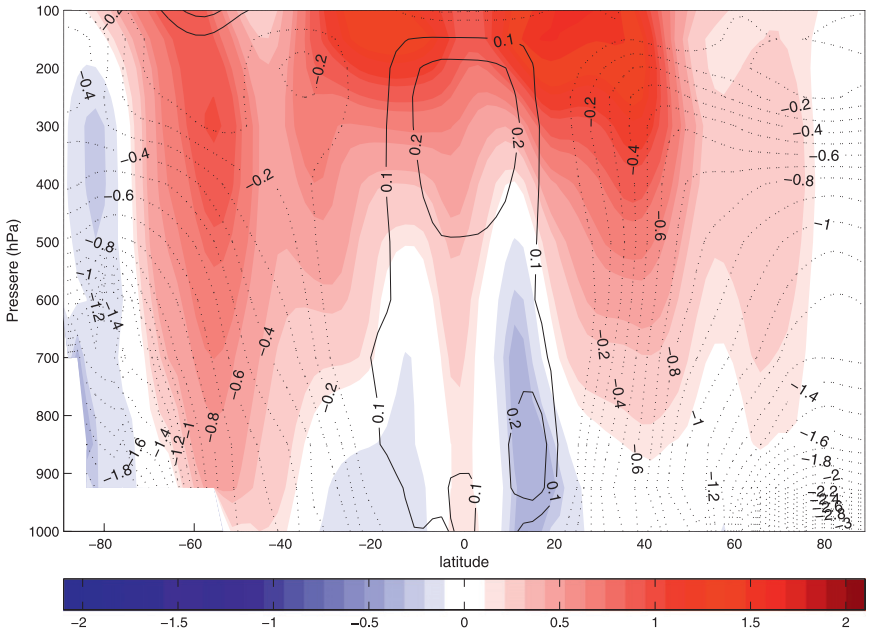

FIG. 2. Annual mean changes (low − high obliquity) of zonal mean temperature (°C, contours) and zonal average of zonal wind (m s^{-1}, colors).

FOAM had a weaker surface temperature response (global cooling of −0.12°C; S.-Y. Lee 2009, personal communication), with the positive SST anomalies extending almost across 30°N−30°S in a much more zonally homogenous way, compared with our results. This suggests that processes operating in the eastern ocean basins, such as the response of low clouds and ocean circulation (described in the following sections), resulted in a different simulation of the climate response to obliquity between the two models.

4. Atmosphere–ocean circulation and heat transports

The contrast between the radiative gain in the tropics and the radiative loss at high latitudes caused by the meridional gradient of the solar radiation is balanced in part by the atmospheric–oceanic general circulation that transports heat from the tropics to high latitudes. Therefore, it is reasonable to expect an intensification of the zonal mean circulation and the associated heat transports as the meridional gradient of the insolation and this radiative contrast increase.

As the meridional temperature gradient increases, the westerly winds also strengthen in agreement with the thermal wind relation (Rind 1998), with the largest increase in the upper troposphere (Fig. 2). The zonal mean Hadley circulation also intensifies by approximately 5% (Fig. 3a). The intertropical convergence zone (ITCZ), which is associated with the rising branch of the Hadley circulation, intensifies, and the subtropical dry regions, which are associated with the descending branches of the Hadley circulation, get even drier (Fig. 3b). This change in zonal mean meridional circulation also appears in the sea level pressure (SLP) field as a strengthening of the high-pressure belts over the subtropics, particularly in the eastern part of the basins (Fig. 4). The poleward atmospheric heat transport also increases (Fig. 3c). In the tropics, this can be attributed to the increase in the Hadley circulation and the zonal mean meridional temperature, humidity, and geopotential gradients as well; however, in the extratropics, this is caused by an increase in eddy activity (stationary and transient). This increase in eddy activity is consistent with increased baroclinicity in the subtropics and midlatitudes, measured by the vertical shear of the zonal wind and the meridional temperature gradient (Fig. 2), the anomalous midlatitude Ferrell circulation (Fig. 3a) (which represents the circulation response to the northward heat flux associated with the midlatitude eddy activity), and the increase in large-scale midlatitude precipitation (Fig. 3b). However, this increase in large-scale precipitation does not result in an increase of total precipitation in the extratropics because of the reduction of convective precipitation (Fig. 3b), which is the result of both the surface cooling and the stabilization of the atmospheric column. The stabilization occurs because the cooling is greater at low levels than aloft.

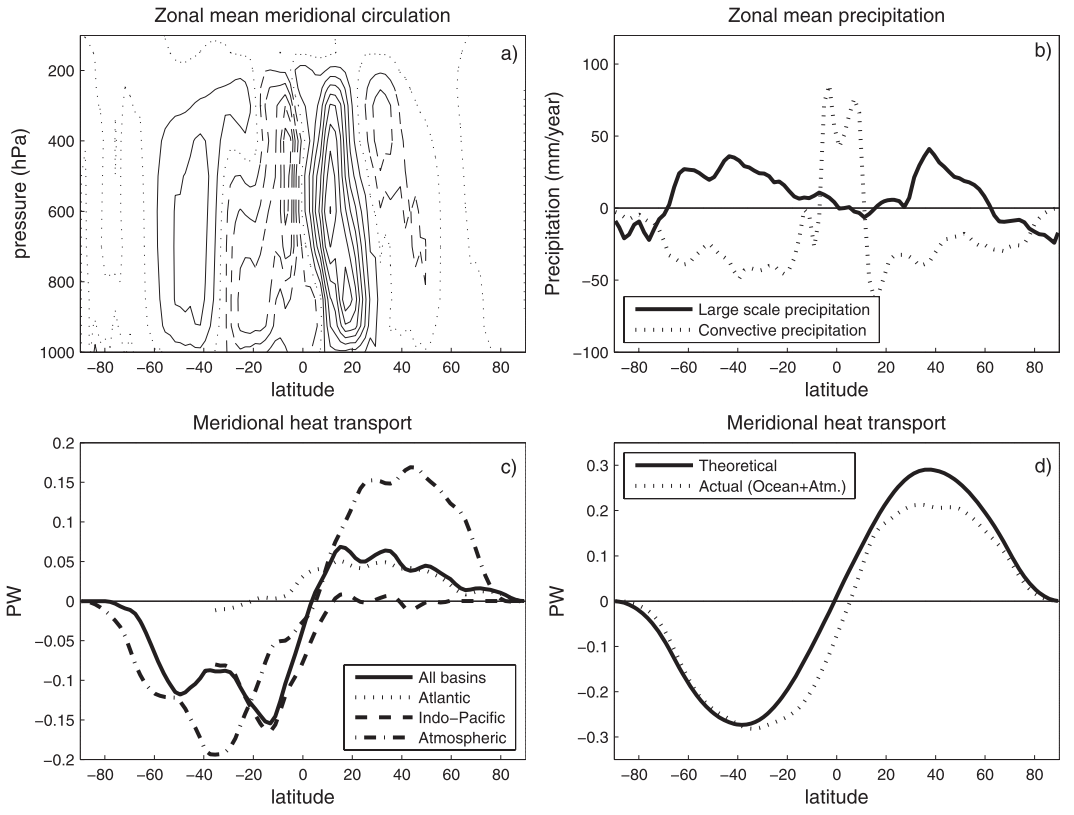

FIG. 3. Annual mean changes (low − high obliquity) for (a) the zonal mean meridional circulation (contours, 10^9 kg s^{-1}), (b) zonal mean large-scale and convective precipitation, (c) atmospheric and ocean (by basin) heat transports (PW), and (d) theoretical and actual total heat transports (PW). Heat transports were calculated by spherical integration of TOA and surface fluxes.

The ocean heat transport also increases; however, unlike the atmospheric heat transport, this increase is asymmetric in the two hemispheres (Fig. 3c). In the Southern Hemisphere, the increase in the ocean heat transport occurs in the Pacific and Indian Ocean basins; and in the tropics is larger than the atmospheric heat transport increase. In contrast, the change in ocean heat transport in the Northern Hemisphere is smaller, and it takes place in the Atlantic basin with a small cross-equatorial component. Also, notice that the ocean and atmospheric heat transport have the same sign and do not partially compensate each other. These findings agree with the Antarctica deuterium-excess records, which show that periods of reduced obliquity are associated with increased ocean heat transport in the Southern Hemisphere (Vimeux et al. 1999).

Another aspect of the general ocean–atmosphere circulation is its effectiveness in balancing the TOA insolation change (also called insolation forcing). Part of the insolation change will be reflected back to space as a result of the planetary albedo, even without any changes in Earth's albedo, and the remaining part represents the radiative forcing. A global integration of the radiative forcing gives the "theoretical" total heat transport, which represents what the ocean–atmosphere heat transport would be if it were 100% efficient and completely balanced the radiative forcing alone, without the additional contribution from local fluxes. Therefore, the difference between the theoretical and the actual heat transports gives us the part of the radiative forcing that is balanced locally by radiative fluxes (in units of PW), as a result of climate feedbacks (clouds, water vapor, surface albedo, temperature). Figure 3d tells us that, in the Southern Hemisphere, from 90°S to 60°S, as well as most of the Northern Hemisphere, the ocean–atmosphere system balances a large fraction of the change in the radiative forcing through heat transport. Local radiative fluxes, associated with feedbacks, balance a smaller part of the radiative forcing, with the biggest contribution north of the equator and in the northern midlatitudes. Conversely, in the low and midlatitudes of the Southern Hemisphere, the actual heat transport overwhelms the theoretical heat transport, and the local feedbacks work against the heat transport to balance the change in the

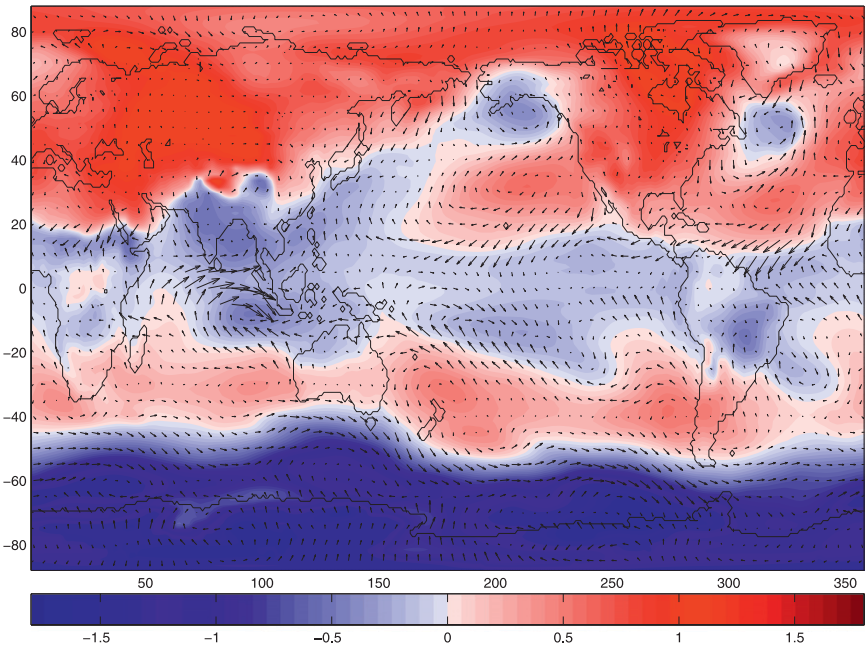

FIG. 4. Annual mean changes (low − high obliquity) of surface wind vectors (at 10-m reference height) and surface pressure (hPa).

radiative forcing. This is associated with a change in the cross-equatorial total heat transport from the Northern to the Southern Hemisphere. The climatology of this model consists of a positive (northward) cross-equatorial total heat transport, and low-obliquity conditions tend to reduce this asymmetry in the total ocean heat transport.

Another useful diagnostic of climate change is the change in net surface heat flux Q_{NET} (Fig. 5a), which, in a climate in equilibrium, has to be balanced by changes in ocean temperature advection. A heat budget analysis (Fig. 5) shows how the horizontal–vertical advection of resolved currents and the diffusion of subgrid-scale processes of the first 75 m of the upper ocean balance the changes in Q_{NET} (results are not sensitive to the depth of integration up to 155 m). Details on how the heat budget analysis is computed can be found in DiNezio et al. (2009). In much of the tropical oceans, vertical heat transport cools the ocean surface layer (Fig. 5b) because of a strengthening of the vertical temperature gradient and increased upwelling induced by the surface wind field. Another notable feature is the warming due to the increased horizontal advection in the western boundary currents (such as the East Australian and Angulhas Currents, Kuroshio, and the Gulf Stream), attributed to changes of the intensity of the western boundary currents (WBCs) (Fig. 5c). Indeed, the surface pressure field is consistent with an intensification of the gyre circulation in the Indian Ocean, South and North Pacific, and the North Atlantic, which would cause an intensification of the WBC, explaining to a large extent the changes in the ocean heat transport in the midlatitudes. Also, in the Northern Hemisphere, the increase of meridional heat transport that mostly takes place near the WBC is also associated with a strengthening of the Atlantic meridional overturning circulation (AMOC) by 1 Sv (1 Sv $\equiv 10^6$ m^3 s^{-1}; not shown), which is rather small compared to the interannual and interdecadal variability of the AMOC in CM2.1 (Delworth et al. 2006).

The 0.12 PW increase in ocean heat transport around 50°S is associated with an intensification of the surface westerly winds at that latitude, which induces more Ekman transport of cold surface water toward the equator (not shown). This is consistent with the warming caused by parameterized eddies generated in the Antarctic Circumpolar Current (Fig. 5d). These eddies travel poleward and are closely associated with the westerly wind anomalies that are a result of the increased atmospheric baroclinic activity.

5. Local radiative feedbacks

The fact that local radiative fluxes are essential in balancing part of the forcing shows that further analysis of radiative feedbacks is required. Two approaches will be used to quantify radiative feedbacks in the obliquity experiments: analysis of clear-sky and total-sky TOA

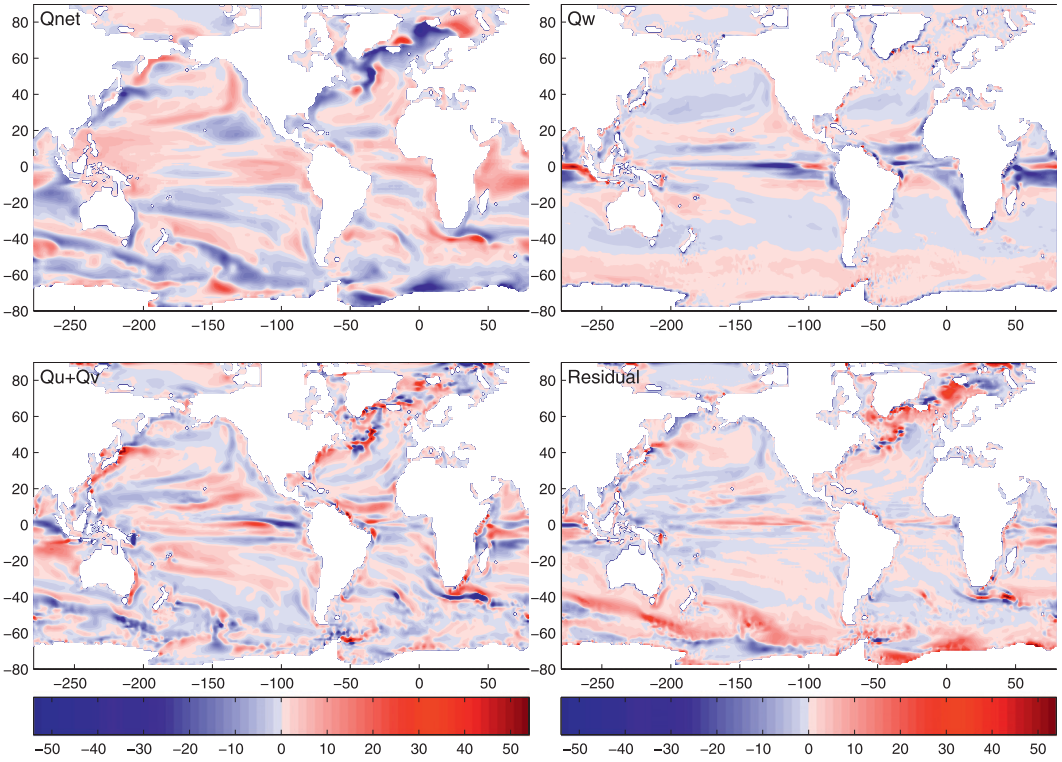

FIG. 5. Surface ocean heat budget analysis as in DiNezio et al. (2009): decomposition of surface net heat flux (Q_{NET}) into horizontal advection ($Q_u + Q_v$), vertical advection (Q_w), and residual (the residual represents the ocean heat transport by subgrid-scale processes). The advection is vertically integrated from the surface to 75-m depth. Values $>\pm 54$ W m^{-2} have been saturated to make the plot clearer. Positive (negative) values represent warming (cooling). Figures represent annual mean changes (low − high obliquity).

fluxes (as in Herweijer et al. 2005), and the radiative Kernel approximation to the partial radiative perturbation method (as in Soden and Held 2006; Soden et al. 2008). Each of these methods has its strengths. The former is simple to compute and utilizes quantities that can be measured from satellite platforms, while the latter can better distinguish among feedback processes and is less subject to the cloud masking biases that can complicate the interpretation of changes in cloud radiative forcing (Soden et al. 2004). The kernel method uses a stand-alone radiation model to calculate a set of radiative kernels representing the response of the TOA radiation balance to unit changes in cloud amount, albedo, temperature, and water vapor. Radiative feedbacks are estimated by multiplying these kernels by the simulated changes in climate variables, reducing the computational expense by eliminating the need to make extensive calculations with the stand-alone radiation model.

The TOA radiative balance requires that changes in the incoming solar radiation be balanced by changes in reflected shortwave (SW) radiation, the temperature-dependent outgoing longwave (LW) radiation (OLR), and a residual (Q_{NET}). Averaged over the globe, this can be written as

$$\Delta Q_{\mathrm{NET}} = \Delta \mathrm{SW}{\downarrow}_{\mathrm{TOA}} - \Delta \mathrm{SW}{\uparrow}_{\mathrm{TOA}} - \Delta \mathrm{OLR}(T). \qquad (1)$$

Assuming global mean conditions, the relationship can be simplified by neglecting the term $\Delta \mathrm{SW}{\downarrow}_{\mathrm{TOA}}$ that has a zero global mean. This means that for a climate in equilibrium, where the global mean of ΔQ_{NET} is zero, an increase (reduction) in the reflected SW radiation has to be balanced by a reduction (increase) in OLR that translates to a reduction (increase) in global mean temperature. We can expand the OLR term by including the greenhouse trapping effect of the atmosphere (G_T), which by definition represents the amount of longwave radiation emitted from the surface that does not escape into space ($G_T = \varepsilon\sigma T_S^4 - \mathrm{OLR}$) because of absorption by atmospheric water vapor and other greenhouse gases and a change in the atmospheric lapse rate (Herweijer et al. 2005). After some manipulation, we can write the change in the surface outgoing longwave radiation as a function of greenhouse trapping, the TOA-reflected SW radiation,

TABLE 1. Annual and global mean changes for each of the radiative components from the TOA radiative equilibrium balance (total, CLR, and CRF components).

Variable (W m^{-2})	CLR	CRF	TOTAL
$\Delta LW\uparrow_{SFC}$	−2.51	0.0	−2.51
ΔOLR	−1.00	0.02	−0.98
ΔG_T	−1.51	−0.02	−1.53
$\Delta SW\uparrow_{TOA}$	0.39	0.64	1.03
ΔQ_{NET}	0.61	−0.66	−0.05

TABLE 2. Annual mean changes (low − high obliquity) of effect of feedbacks on the TOA net radiation as diagnosed from the kernel analysis.

Feedback	Effect on TOA net radiation (W m^{-2})
LR	−0.90
WV	−0.20
Clouds	−0.69
SFC albedo	−0.30
Total	−2.09

and the net radiative flux at the TOA. The last term is close to zero (the fact that ΔQ_{NET} is not zero is associated with the small temperature trends of the deep ocean), and it will be treated as a residual of the radiative balance described as follows:

$$\Delta LW\uparrow_{SFC} = \Delta G_T - \Delta SW\uparrow_{TOA} - \Delta Q_{NET}. \quad (2)$$

Each term of the radiative analysis described above is presented in Table 1 after separating the total component into the clear-sky (CLR) and cloud radiative forcing (CRF) part. Table 1 reveals that the outgoing LW radiation both at the surface and TOA decrease (consistent with a reduction in temperature); however, this is much greater at the surface, and since the difference of these two make up the atmospheric greenhouse effect, this means that the ability of the atmosphere to trap the outgoing LW radiation is reduced, and hence the atmosphere cools. The small contribution of the CRF to the reduction of the greenhouse trapping means that the change in clouds has a minimal contribution, at least in the global mean sense. A similar result was found by Braconnot et al. (2007) in Last Glacial Maximum (LGM) experiments, where clouds were found to have a relatively small impact on the TOA radiation budget. Conversely, the CLR component dominates the reduction of the greenhouse trapping effect, and the only way to explain this is through the change in the distribution of the atmospheric water vapor content and the lapse rate (Herweijer et al. 2005). Table 1 also reveals that the global surface cooling can also be attributed to the increase in the outgoing SW_{TOA} radiation. Unlike the reduction in G_T, the increase in the outgoing SW_{TOA} radiation can be attributed to both the CRF (60%) and the CLR (40%) conditions, with CLR implying a change in surface albedo. It should be noted that this heat budget analysis does not take into account the fact that part of the insolation change will be reflected back to space as a result of the planetary albedo, even without any changes in Earth's albedo. However, in the global mean sense this is very small and does not change the results qualitatively.

The feedbacks inferred from the TOA radiation balance are broadly consistent with the results from the kernel analysis (Table 2), in that all of the feedback processes (i.e., lapse rate, water vapor, surface albedo, and clouds) result in negative contributions to the TOA radiation budget (note that the kernel results are presented as the changes in TOA net radiation associated with each feedback process and are not normalized by the change in global surface temperature as is typically done in studies of radiative feedbacks). Only broad consistency between the two methods is expected because both methods only approximate the cloud feedback component. In particular, the TOA radiation balance method has been found to not distinguish between cloud feedback and cloud masking effects (Soden et al. 2004). The lapse rate and cloud feedbacks are largest, and the water vapor and surface albedo feedbacks are considerably smaller. The relative contribution of each feedback process, based on the kernel analysis, is lapse rate (43%), clouds (33%), surface albedo (14%), and water vapor (10%). Although each of these feedback processes reduces the global mean TOA net radiation, their effects vary considerably with latitude, as will be discussed in the following subsections.

a. Greenhouse effect

The overwhelming contribution of the CLR component relative to the CRF part of the total greenhouse trapping (Table 1) implies that the changes in the lapse rate and the WV content of the atmosphere have a significant impact on the outgoing LW radiation. The CLR component of G_T increases in the tropics and reduces everywhere else, similar to the changes in WV content (Fig. 6a). The lapse rate changes and the resulting feedback effect as diagnosed by the kernel analysis (Fig. 6b) are small at low latitudes, allowing the WV warming effect to be dominant. Conversely, the lapse rate changes are very large at higher latitudes, leading to a strong cooling effect. Also, the influence of the WV increase in the tropics on the global mean greenhouse trapping is overwhelmed by the reduction of WV that takes place from the subtropics and poleward.

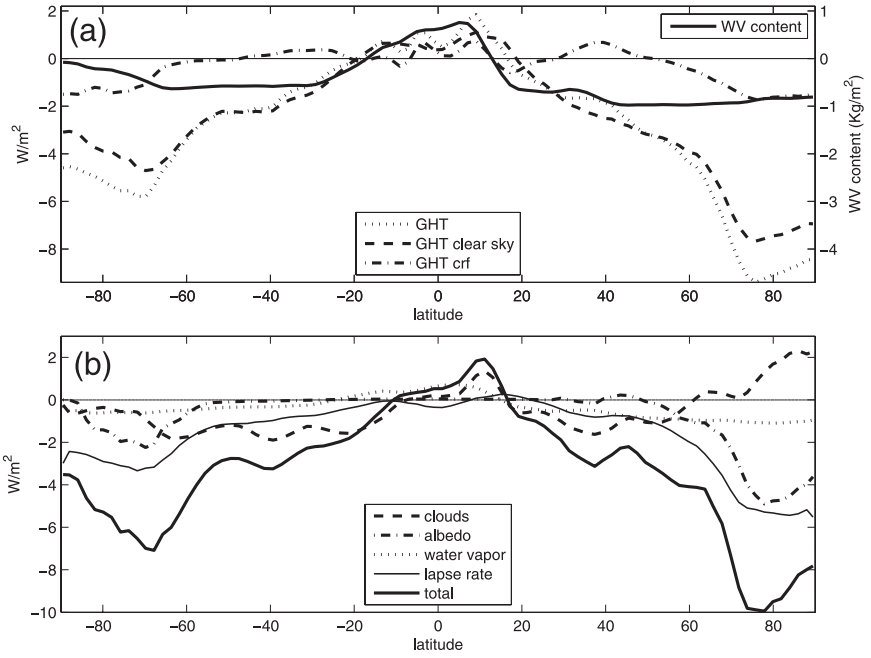

FIG. 6. Annual mean changes (low − high obliquity) for (a) G_T (total, clear sky, and cloud radiative component), and column-integrated atmospheric WV content. (b) Effect of individual feedback processes on zonal mean TOA net radiation, as diagnosed from the kernel method.

The WV changes can be explained by two mechanisms: a direct thermodynamic and an indirect dynamic. The thermodynamic mechanism relates the changes in temperature to those in WV content of the atmosphere through the Clausius–Clapeyron equation. More (less) SW↓ in the tropics (high latitudes) results in an increase (reduction) in the temperature. If the relative humidity is constant, this implies an increase (decrease) in the specific humidity that increases (reduces) the G_T, constituting a positive feedback on the temperature. Indeed, the meridional T distribution resembles that of the WV content.

However, circulation changes can also alter the WV distribution (dynamic effect) and hence the G_T (i.e., Herweijer et al. 2005). A simple way to quantify the relative influence of the thermodynamics is to examine the specific humidity change given a fixed relative humidity (Fig. 7a) and subtract that from the actual humidity change (Fig. 7b). The residual can be roughly attributed to dynamics (Fig. 7c) (Stephens 1990).

Despite the dynamical part of the change in specific humidity dq providing a feedback on the temperature (through its G_T effect)—which was used for the separation in the first place—the changes in the circulation are consistent with the changes in the dynamical part of dq. This is apparent in the relative humidity distribution (Fig. 7d). In the deep tropics, where we have increased ascending motion, the relative humidity increases; however, in the subtropics and especially in the Northern Hemisphere, the anomalous descending motion reduces the relative humidity. A comparison of these two processes reveals that the thermodynamic component is larger at high latitudes; however, at low latitudes the dynamical part has a comparable effect, especially in the northern subtropics.

b. Cloud effect

As presented in Tables 1 and 2, roughly two-thirds of the increase in the $\mathrm{SW}{\uparrow}_{\mathrm{TOA}}$ is related to changes in clouds. Indeed, all cloud types experience an increase in zonal mean cloud fraction at most latitudes (Fig. 8a). Only at high latitudes (especially in the Northern Hemisphere), despite the increase in total cloud cover, is there a large increase in net radiation from cloud feedback (Fig. 7b), as a result of a dramatic change in cloud optical properties (i.e., reduction of cloud liquid water and ice content due to the decrease in temperature).

Among cloud types, low clouds experience the highest increase everywhere except the deep tropics (5°S–15°N), where changes in high cloud cover dominate (Fig. 8a). The effect of middle and, most particularly, high clouds on the $\mathrm{SW}{\uparrow}_{\mathrm{TOA}}$ is largely offset by their effect on the OLR, making low clouds have the largest impact on the TOA Q_{NET}.

The increase in low cloud fraction is largest in the five marine subtropical stratus regions (Californian, Peruvian,

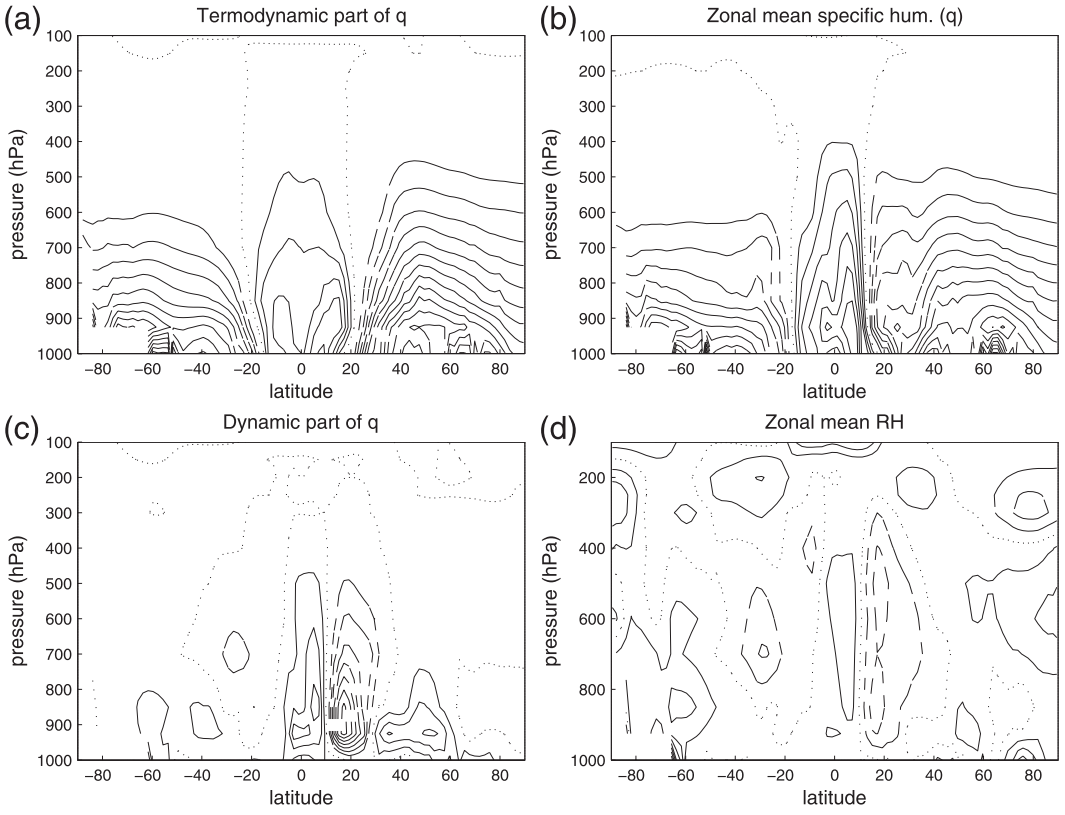

FIG. 7. Annual mean changes (low − high obliquity) of (a) thermodynamic part of specific humidity, (b) actual specific humidity, (c) dynamic part of specific humidity, and the (d) relative humidity (%).

Canarian, Namibian, and Australian), the North Pacific and North Atlantic stratus regions, and the circumpolar stratus region, where we see the biggest changes (Fig. 8b). The increase in the low cloud fraction in the eastern subtropical basins is associated with the reduction of SST in these regions and the increase of the zonal SST gradient, mentioned in section 3. But, what is the cause of this increase in low cloud fraction?

It is well known that when the strength of the inversion layer that caps the planetary boundary layer (PBL) increases, it becomes more effective in trapping the moisture in the marine BL, allowing more low clouds to form (Klein and Hartmann 1993). A measure of the strength of this inversion layer is the estimated inversion strength (EIS), defined by Wood and Bretherton (2006) as

$$\mathrm{EIS} = \theta_{700} - \mathrm{SST} - \Gamma_{\mathrm{m}}^{850}(z_{700} - \mathrm{LCL}), \qquad (3)$$

where the first two terms represent the lower-tropospheric static stability (LTS) introduced by Klein and Hartmann (1993). The third term constitutes a small correction based on the general observation that the free tropospheric temperature profile that caps the PBL is often close to a temperature-dependent moist adiabatic lapse rate, and practically accounts for any changes in temperature. The lifting condensation level (LCL) was calculated using surface values of temperature and relative humidity as suggested by Bolton (1980).

Figure 10c shows that the LTS is increasing over the entire ocean, indicating that ($d\theta_{700} > d\mathrm{SST}$) and that the lower troposphere becomes more stable. However, this increase is small at around latitude 50° in both hemispheres. This means that the changes in the LTS alone cannot explain the changes in marine low cloud fraction, as seen by the increase in the low clouds in the extratropics (Figs. 8a,b), and the additional effect of the moist lapse rate term needs to be investigated. According to Eq. (3), in the tropics (25°S–22°N), the change in the moist adiabatic lapse rate term opposes the change in LTS, and it tends to destabilize the lower troposphere (Fig. 8c). Conversely, outside the tropics, this term tends to stabilize the lower troposphere, with a greater magnitude at higher latitudes. Particularly in the subtropical regions (around 20°N and 20°S), where stratocumulus decks develop, the LTS increase overwhelms the effect of the lapse rate. The result is that the EIS increases in the tropics as well as in the extratropics (Figs. 8c,d), and it agrees with the changes in low cloud fraction (the spatial correlation

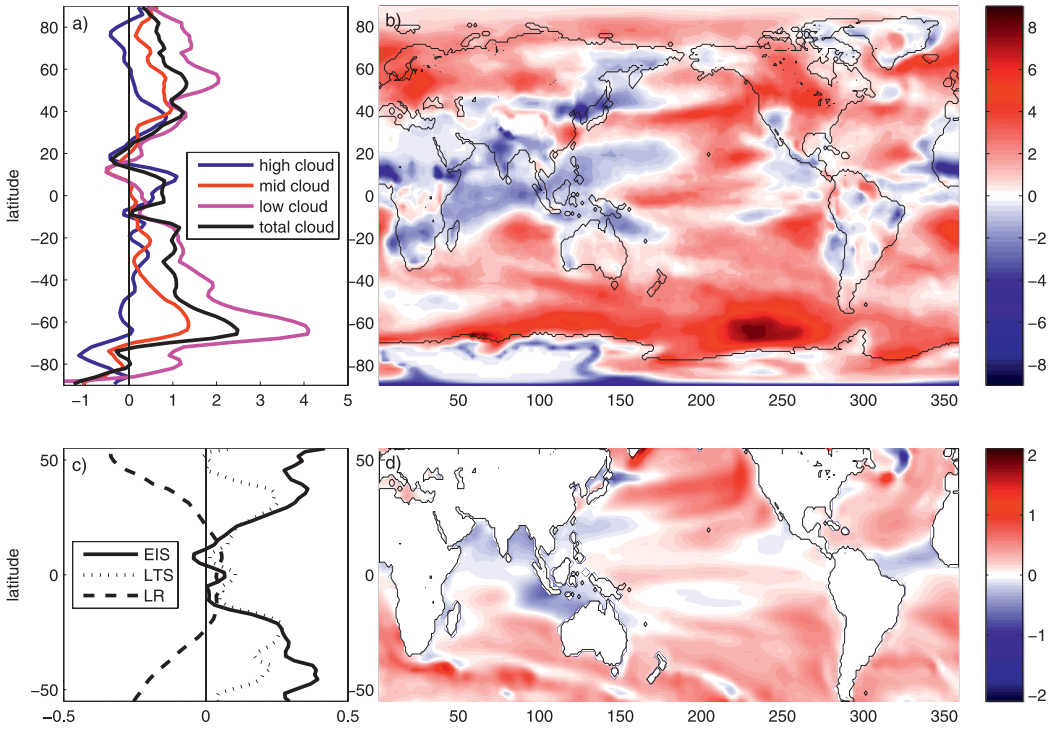

FIG. 8. Annual mean changes (low − high obliquity) in (a) zonal mean cloud fraction cover (%) for all cloud types. (b) Low cloud fraction cover (%). (c) Zonal mean EIS, LTS, and LR effect over ocean. (d) EIS over ocean (values >2.1 have been saturated to make the figure clearer).

over ocean from 55°S to 55°N is 0.54), which constitute the biggest contribution to the $SW\uparrow_{TOA}$, as mentioned above.

This analysis indicates that the cloud cover change in this model is consistent with the change in inversion strength, as it is in observations. Why does the inversion strength change in this way? This is difficult to unravel, because the inversion strength is influenced by both thermodynamic and dynamic processes, and there is also a feedback between the two. For example, a decrease in surface temperature in the eastern subtropics can on its own increase the lower tropospheric stability, and one would then expect an increase in cloud cover (i.e., a positive feedback) (Klein and Hartmann 1993). However, a decrease in surface temperature in the subtropics would also strengthen the subtropical high, and the associated circulation, from which one would also predict an increase in inversion strength and an increase in cloud cover (Ma et al. 1996; Misra and Marx 2007; Nigam 1997; Norris 2005; Wang et al. 2005). In other words, there is a positive feedback among clouds, temperature, and circulation, as discussed in Clement et al. (2009). It appears that a similar positive feedback operates in this model in response to obliquity forcing and that in the subtropics, this feedback, at least in part, overwhelms the direct radiative forcing. That is, while the direct radiative forcing would result in an increase in temperature, there is instead a decrease in temperature, and an increase in cloud cover and strengthened subtropical highs (Fig. 4). This suggests that the temperature in those regions is more strongly dominated by remote dynamical influences (such as the strengthened Hadley circulation) than it is by local adjustment to the forcing.

Unlike low clouds, the largest changes of high cloud cover are located in the tropics (Fig. 8a). Increases (reduction) in high cloud cover in the tropics are associated with an increase (reduction) in convective activity. For midclouds the largest changes are associated with large-scale precipitation taking place at midlatitudes and can be explained by the increase in eddy activity, as seen in section 4. Some of the changes in low cloud cover can also be attributed to this eddy activity, especially over North America, the North Atlantic, Europe, and the northeastern Pacific.

c. *Surface albedo effect*

Tables 1 and 2 show that changes in surface albedo at high latitudes account for roughly one-third of the increase in the reflected SW_{TOA} radiation. The largest albedo effect is provided by an increase of the annual sea ice fraction (Fig. 9a), which in the Northern Hemisphere is located in the Arctic region and around Greenland as

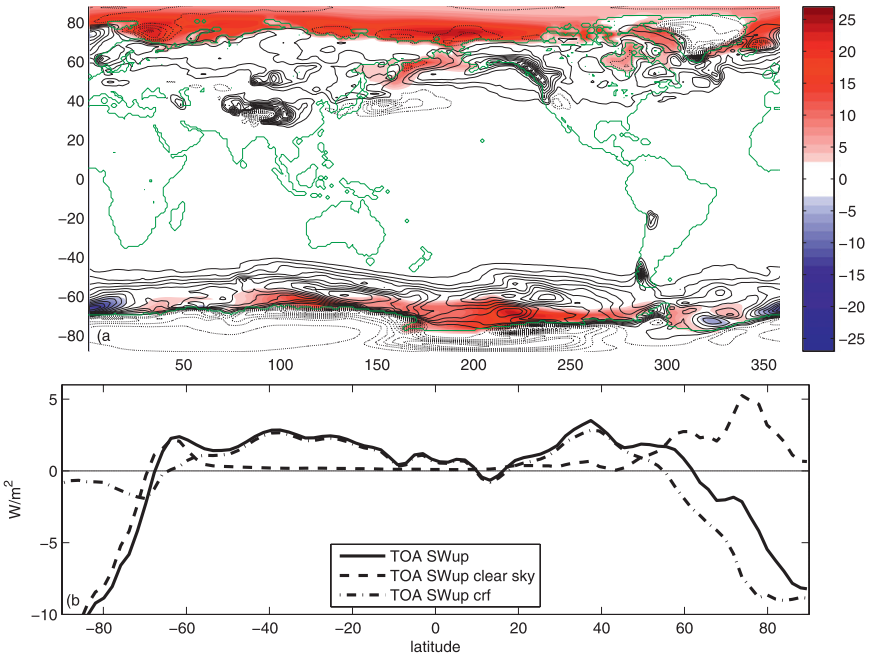

FIG. 9. Annual mean changes (low − high obliquity) in (a) sea ice fraction (%, colors) and annual snowfall (contours, 10 kg m^{-2}), and (b) zonal-mean-reflected TOA SW radiation (clear sky, cloud radiative forcing, and total component, W m^{-2}).

well as the northeastern coast of the Pacific and Atlantic basins. In the Southern Hemisphere, the ice fraction increases around the Antarctic Peninsula, primarily in the Indian and Pacific sectors. The surface albedo also changes because of changes in the snowfall over land, mostly in the Northern Hemisphere (Fig. 9a). In general, there is more snowfall in high latitudes, which increases the surface reflection of SW radiation. Only high-latitude areas with high elevation, like Greenland and Antarctica, exhibit reduced snowfall. Also, over high-latitude areas covered by permanent ice sheets, such as Antarctica and Greenland, where the albedo does not change, the reduction of reflected SW radiation is the result of the reduction of incoming SW radiation because of orbital forcing (Fig. 9b).

6. Comparison with available proxy record

In contrast with the available proxy record, which provides evidence of tropical cooling ranging roughly from 1° to 2°C, when obliquity-induced local insolation is stronger, the GFDL model exhibits only a slight surface annual mean cooling in parts of the tropics. In many other parts of the tropics, it predicts a small warming, similar to results from FOAM (Lee and Poulsen 2005). Several factors could lead to this discrepancy.

One issue is uncertainties in the temperature records derived from alkenone and foraminifera productivity. The productivity of such proxies often has a seasonal maximum (Herbert 2003), and it is not representative of the annual mean. This is because it depends on upwelling-induced nutrient availability, which is strongly seasonal. Since upwelling is associated with cooling, this means that tropical SSTs based on alkenone or foraminifera productivity could be biased toward colder temperatures, as addressed by Cleaveland and Herbert (2007). On a seasonal time scale, the GFDL model shows that the tropical SSTs can be slightly cooler in some seasons, despite the stronger insolation (Fig. 10a). This depends on the region; however, it includes the sites in the east Pacific [Ocean Drilling Program (ODP 846)], west Pacific (Hole 806B), and east Atlantic (ODP 662), from which some of the temperature paleorecord comes. If the proxies are seasonally biased, then this could partly resolve the discrepancy with the model simulation.

Also, it is important to note that the number of sites that document the SST variability during the late Pliocene and early Pleistocene is limited, and proxies from additional sites would improve our understanding regarding the extent of tropical cooling when Earth's axial tilt is reduced.

Ambiguities also exist on the depth that the alkenones and the foraminifera represent. Alkenone maximum productivity is not always located at the surface layer, and it can be located around 50-m depth or even deeper in some regions. Also, vertical migration of foraminifera

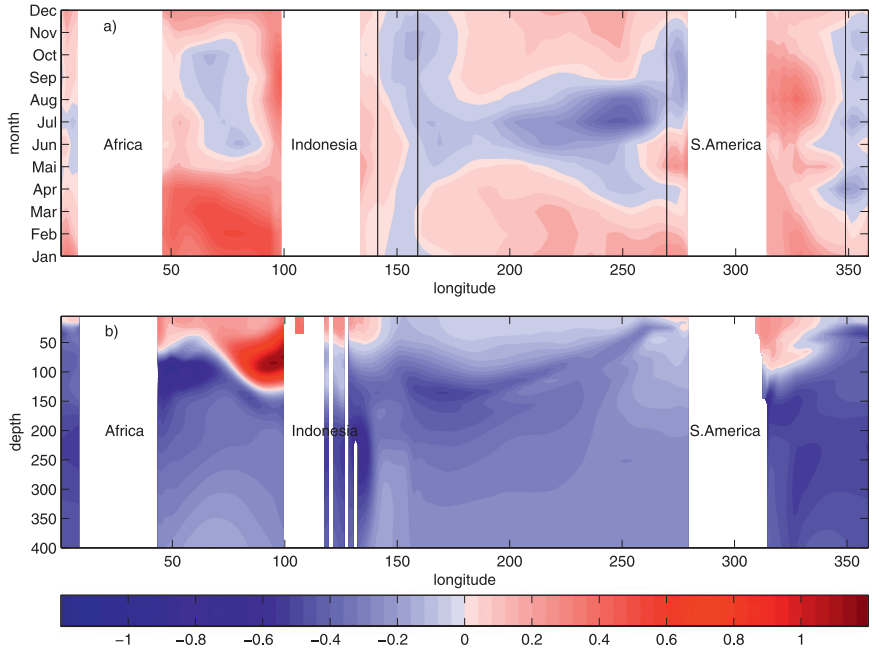

FIG. 10. (a) Change (low − high obliquity) in the seasonal cycle of the tropical SSTs (average from 5°S to 5°N) as a function of longitude. White areas represent areas where land dominates. Black lines represent the longitude where ODP sites 846, 662 (Cleaveland and Herbert 2007), 806B, and MD97–2140 (Medina-Elizalde and Lea 2005) are located (all sites are located close to the equator). (b) Annual mean change (low − high obliquity) in equatorial temperature depth profile (5–400 m).

and the addition of calcite on their shell at the end of their life span question the ocean depth that the Mg/Ca ratio represents (Lea 2003). Furthermore, postdeposition processes can also affect the Mg/Ca ratios, making the interpretation of such proxies even harder (Lea 2003). Lee and Poulsen (2005) showed that the simulated tropical average temperature change of the 30–100-m layer, between low- and high-obliquity conditions, has the opposite sign compared to the SSTs. Our study also shows that the GFDL model exhibits a cooling on the equator for the same layer in the entire Pacific basin as well as the central and east Atlantic basins (Fig. 10b). If the alkenone-based SSTs represent a deeper layer, instead of the SSTs, then this could seriously bias the interpretation of the alkenone productivity, leading to a counterintuitive result.

Conversely, it is possible that the model simulation underestimates the cooling of the tropical SST in response to reduced obliquity. In the polar regions, the insolation decreases by 10%, which could directly affect the surface temperatures; however, in the tropics, the insolation increases less than 1%, and dynamical processes or feedbacks could easily overwhelm the direct solar forcing. In particular, so-called slow feedbacks involving ice sheets and atmospheric greenhouse concentrations are not included in the experimental design.

The influence of Northern Hemisphere ice sheets is not simulated because ice sheets were kept constant. However, studies with atmospheric models coupled to slab ocean models (Broccoli and Manabe 1987; Chiang and Bitz 2005) and fully coupled models (Shin et al. 2003; Otto-Bliesner et al. 2009) show that Northern Hemisphere ice sheets of the LGM, besides cooling the high latitudes, can also slightly cool the tropics. However, Lisiecki and Raymo (2005) showed that the cycles in global ice volume, as measured by the benthic $\delta^{18}O$, during the 41-kyr world, were roughly half compared to those of the late Pleistocene, implying that the associated radiative forcing of the ice sheets was also smaller.

Another limitation of these experiments is that the atmospheric CO_2 was kept constant. It is well documented that CO_2 concentrations were increased (reduced) during interglacial (glacial) periods over the last 800 kyr (Petit et al. 1999). Recent modeling studies (Broccoli and Manabe 1987; Shin et al. 2003; Otto-Bliesner et al. 2009) showed that the variability of CO_2 operating during the glacial–interglacial cycles of the late Pleistocene (100-kyr world) accounts for roughly 50% of the simulated cooling in the tropics. Khodri et al.

(2009) estimated that the greenhouse effect of reduced CO_2 during the LGM was even greater, accounting for almost the entire tropical cooling, as opposed to a small effect from ice sheets. Unfortunately, the available proxy record that documents the variability of the atmospheric CO_2 does not cover the late Pliocene and early Pleistocene (41-kyr world); however, a similar CO_2 feedback operating during that period cannot be ruled out. Low-obliquity periods could be associated with global cooling, including the tropics, because of reduced atmospheric CO_2, which could amplify the effect of increased glaciation. Further development of proxies of CO_2 is necessary to resolve this issue.

The experiments presented here cannot provide a quantitative test of the effects of ice sheets and CO_2 on tropical cooling since both were kept constant, but future experiments that would test this idea are under development. However, a simple argument can be made that inclusion of the effect of CO_2 and ice sheets could bring the model simulations and paleo-observations into agreement. Jouzel et al. (2007) estimated the GHG radiative forcing for the largest obliquity swings at roughly 0.6 W m^{-2}. Also, the radiative forcing for the LGM ice sheets has been estimated to be 2–3 W m^{-2} (Taylor et al. 2007). This means that for the 41-kyr cycles, where the ice volume maximum was roughly half (Lisiecki and Raymo 2005), the combined radiative forcing of the ice sheets and GHGs could be estimated at around a 1.5–2 W m^{-2} reduction (global means), and together with the climate feedbacks, it is more than enough to increase the cooling throughout the tropics. The way in which CO_2 is drawn down in response to obliquity, however, is unknown. Toggweiler et al. (2006) has suggested that changes in the Southern Ocean MOC cause changes in the ventilation of CO_2 out of the deep ocean. Taken at face value, one would predict an increase in CO_2 for low obliquity based on the strengthening of the MOC. Model experiments with an interactive carbon cycle could be used to test these ideas.

Besides the tropics, our experiments also underestimate the surface cooling in the extratropics, which, according to Lawrence et al. (2010), would range between 2° and 4°C in the North Atlantic, and the explanation could be similar (regarding CO_2 concentrations and continental ice sheets that were not included in our experiments).

Despite that the model fails to reproduce the strong tropical cooling when obliquity is low, it also shows a zonal SST gradient in the subtropical oceans, which can be partly attributed to changes in ocean circulation and low cloud feedback as well. A comparison of proxy data from the eastern and western subtropical Pacific (currently not available) could test whether such mechanisms are supported by the available proxy record and whether these simulations are realistic.

7. Discussion and conclusions

The reduction in Earth's axial tilt, used for this study, enhances the radiative contrast between low and high latitudes. The coupled system responds by strengthening the zonal mean meridional atmosphere and ocean circulation and increases the poleward heat transport. The changes in the heat transport balance most of the radiative forcing, and the remaining part is balanced locally by radiative fluxes, where climate feedbacks (clouds, water vapor, lapse rate, and surface albedo) play an important role. All climate feedbacks have a global cooling effect, even though their relative effects vary considerably with latitude. Among feedbacks, clouds and lapse rate have the larger contribution, with water vapor and surface albedo having a smaller effect. Among clouds, low clouds account for the biggest feedback. Our analysis shows that the marine low cloud coverage increases because of the strengthening of the inversion strength at the top of the marine boundary layer, which is not directly driven by the changes in the insolation but rather the result of feedbacks.

Unlike high and middle clouds, low clouds contribute negatively to the NET_{TOA} radiation, by reflecting more SW↓ than trapping the LW↑ radiation, and they have a cooling effect on climate (Hartmann et al. 1992). Despite the small sensitivity of LW↑ and SW↓ to low clouds, low clouds compensate with their abundance, which also explains why they have the biggest effect on the incoming SW radiation. Unfortunately, clouds provide the largest source of uncertainty in current model prediction of climate sensitivity (Soden and Held 2006), because of uncertainties in the cloud parameterization schemes being different for each model, which in general questions the robustness of the cloud response and its effect on the energy budget. Perhaps paleoclimate records from the subtropics could shed some light on the strength of low cloud feedbacks in the real world.

The strengthening of the radiative gradient between low and high latitudes due to the reduction in Earth's axial tilt is a concept with possible implications in the glacial cycles during the 41-kyr world [~(3.0–0.8) Ma ago]. The importance of the gradient to the duration of ice ages was highlighted by Raymo and Nisancioglu (2003). They argued that the Milankovitch hypothesis, according to which global ice volume is controlled by the high-latitude summer insolation, cannot explain climate changes during the 41-kyr world. This is because during that period, the global ice volume varied on the obliquity frequency, unlike the summer high-latitude insolation

that varies on the precessional frequency. However, the summer meridional insolation gradient and its effect on the atmospheric circulation, as well as the northward moisture fluxes that are vital for ice sheet growth, vary at the obliquity frequency (Vimeux et al. 1999; Raymo and Nisancioglu 2003) and together with the integrated total summer insolation, which varies at the same frequency (Huybers 2006), they may explain orbitally driven climate changes before the mid-Pleistocene transition.

Also, according to Philander and Fedorov (2003), the increase in Q_{NET} loss of the ocean near the western boundary currents in high latitudes under low-obliquity conditions should be balanced by the gain of heat at low latitudes and especially in the equatorial upwelling regions. Also, according to the same study, for the tropics this should be associated with a shoaling of the thermocline, increased upwelling in the eastern part of the Pacific and Atlantic basins, reduced SSTs, and increased meridional ocean heat transport from low to high latitudes. This argument was based on experiments with an ocean model forced with winds. In a coupled configuration, as shown here, the ocean does lose more heat to the atmosphere near the western boundary currents and gains heat in the equatorial and costal upwelling regions of the low latitudes (Fig. 5a), and it transports more heat poleward. Furthermore, the eastern sides of the tropical basins experience a reduction in SSTs and the thermocline rises, in most of the tropics, with the exception of the west Pacific (not shown). However, this tropical cooling is weak and some areas—such as in the Indian, west Pacific, and west Atlantic—even experience a slight warming. The changes in thermocline depth, defined as the maximum of the vertical temperature gradient, are very small (the thermocline rising not more than a few meters); however, these changes resemble qualitatively the response mechanism described by Philander and Fedorov (2003). One reason why the coupled response is not as strong as the forced ocean response is that the atmosphere accounts for most of the heat transport. Additionally, climate feedbacks and changes in the atmospheric circulation can alter the response of the surface heat budget (Q_{NET}) to the orbital forcing, which then would limit the applicability of the ocean-only experiments.

The 1°–2°C cooling observed in tropical oceans and the 2°–4°C cooling observed in the North Atlantic, during the late Pliocene and early Pleistocene, when Earth's axial tilt was reduced, could not be reproduced in our experiments by simply reducing the equator-to-pole TOA insolation contrast in association with a reduction in obliquity. Other processes, such as increased Northern Hemisphere ice sheet extent and reduced greenhouse concentrations, could be responsible. Additional experiments that include these processes could bring models and observations into agreement.

Acknowledgments. This research was supported by the NSF Paleoclimate Program (Grant ATM0902926). We are grateful to Dr. R. J. Toggweiler for his useful comments on the CO_2 cycles, and to four anonymous reviewers for their valuable comments and their contribution to improving this article.

REFERENCES

Berger, A., and M. F. Loutre, 1991: Insolation values for the climate of the last 10 million years. *Quat. Sci. Rev.,* **10,** 297–317.

Bolton, D., 1980: The computation of equivalent potential temperature. *J. Climate,* **108,** 1046–1053.

Braconnot, P., and Coauthors, 2007: Results of PMIP2 coupled simulations of the mid-Holocene and Last Glacial Maximum—Part 2: Feedbacks with emphasis on the location of the ITCZ and mid- and high latitudes heat budget. *Climate Past,* **3,** 279–296.

Broccoli, A. J., and S. Manabe, 1987: The influence of continental ice, CO_2, and land albedo on the climate of the Last Glacial Maximum. *Climate Dyn.,* **1,** 87–99.

Chiang, J. C. H., and C. M. Bitz, 2005: Influence of high latitude ice cover on the marine intertropical convergence zone. *Climate Dyn.,* **25,** 477–496.

Cleaveland, C. L., and T. D. Herbert, 2007: Coherent obliquity band and heterogeneous precession band responses in early Pleistocene tropical sea surface temperatures. *Paleoceanography,* **22,** PA2216, doi:10.1029/2006PA001370.

Clement, C. A., R. Burgman, and J. R. Norris, 2009: Observational and model evidence for positive low-level cloud feedbacks. *Science,* **325,** 460–464.

de Garidel-Thoron, T., Y. Rosenthal, F. Bassinot, and L. Beaufort, 2005: Stable sea surface temperature in the western Pacific warm pool over the past 1.75 million years. *Nature,* **433,** 294–298.

Delworth, T. L., and Coauthors, 2006: GFDL's CM2 global coupled climate models. Part I: Formulation and simulation characteristics. *J. Climate,* **19,** 643–674.

DiNezio, P., A. Clement, G. Vecchi, B. Soden, B. Kirtman, and S.-K. Lee, 2009: Climate response of the equatorial Pacific to global warming. *J. Climate,* **22,** 4873–4892.

Dwyer, G. S., T. M. Cronin, P. A. Baker, M. E. Raymo, J. S. Buzas, and T. Correge, 1995: North Atlantic deepwater temperature change during late Pliocene and late Quaternary climatic cycles. *Science,* **270,** 1347–1351.

GFDL Global Atmospheric Model Development Team, 2004: The new GFDL global atmosphere and land model AM2–LM2: Evaluation with prescribed SST simulations. *J. Climate,* **17,** 4641–4673.

Gnanadesikan, A., and Coauthors, 2006: GFDL's CM2 global coupled climate models. Part II: The baseline ocean simulation. *J. Climate,* **19,** 675–697.

Hartmann, L. D., M. E. Ockert-Bell, and M. L. Michelsen, 1992: The effect of cloud type on earth's energy balance: Global analysis. *J. Climate,* **5,** 1281–1304.

Herbert, T. D., 2003: Alkenone paleotemperature determinations. *Treatise Geochem.,* **6,** 391–432.

Herweijer, C., R. Seager, M. Winton, and A. Clement, 2005: Why ocean heat transport warms the global mean climate. *Tellus,* **57A,** 662–675.

Hewitt, C. D., and J. F. B. Mitchell, 1998: A fully coupled GCM simulation of the climate of the mid-Holocene. *Geophys. Res. Lett.,* **25,** 361–364.

Huybers, P., 2006: Early Pleistocene glacial cycles and the integrated summer insolation forcing. *Science,* **313,** 508–511.

Jouzel, J., and Coauthors, 2007: Orbital and millennial Antarctic climate variability over the past 800,000 years. *Science,* **317,** 793–796.

Khodri, M., M. Kageyama, and D. M. Roche, 2009: Sensitivity of South America tropical climate to Last Glacial Maximum boundary conditions: Focus on teleconnections with tropics and extratropics. *Dev. Paleoenviron. Res.,* **14,** 231–238.

Klein, A. S., and D. L. Hartmann, 1993: The seasonal cycle of low stratiform clouds. *J. Climate,* **6,** 1587–1606.

Lawrence, K. T., Z. Liu, and T. D. Herbert, 2006: Evolution of the eastern tropical Pacific through Plio-Pleistocene glaciation. *Science,* **312,** 79–83.

——, S. Sosdian, H. E. White, and Y. Rosenthal, 2010: North Atlantic climate evolution through the Plio-Pleistocene climate transitions. *Earth Planet. Sci. Lett.,* **300,** 329–342.

Lea, D. W., 2003: Elemental and isotopic proxies of past ocean temperatures. *Treatise Geochem.,* **6,** 365–390.

Lee, S.-Y., and C. J. Poulsen, 2005: Tropical Pacific climate response to obliquity forcing in the Pleistocene. *Paleoceanography,* **20,** PA4010, doi:10.1029/2005PA001161.

Lin, S.-J., 2004: A ''vertically Lagrangian'' finite-volume dynamical core for global models. *Mon. Wea. Rev.,* **132,** 2293–2307.

Lisiecki, E. L., and M. E. Raymo, 2005: A Pliocene-Pleistocene stack of 57 globally distributed benthic $\delta^{18}O$ records. *Paleoceanography,* **20,** PA1003, doi:10.1029/2004PA001071.

Liu, Z., and T. D. Herbert, 2004: High-latitude influence on the eastern equatorial Pacific climate in the early Pleistocene epoch. *Nature,* **427,** 720–723.

Ma, C.-C., C. R. Mechoso, A. W. Robertson, and A. Arakawa, 1996: Peruvian stratus clouds and the tropical Pacific circulation: A coupled ocean–atmosphere GCM study. *J. Climate,* **9,** 1635–1645.

Medina-Elizalde, M., and D. W. Lea, 2005: The mid-Pleistocene transition in the tropical Pacific. *Science,* **310,** 1009–1012.

Milly, P. C. D., and A. B. Shmakin, 2002: Global modeling of land water and energy balances. Part I: The land dynamics (LaD) model. *J. Hydrometeor.,* **3,** 283–299.

Misra, V., and L. Marx, 2007: Manifestation of remote response over the equatorial Pacific in a climate model. *J. Geophys. Res.,* **112,** D20105, doi:10.1029/2007JD008597.

Nigam, S., 1997: The annual warm to cold phase transition in the eastern equatorial Pacific: Diagnostics of the role of stratus cloud-top cooling. *J. Climate,* **10,** 2447–2467.

Norris, J. R., 2005: Trends in the upper-level cloud cover and surface divergence over the tropical Indo-Pacific Ocean between 1952 and 1997. *J. Geophys. Res.,* **110,** D21110, doi:10.1029/2005JD006183.

Otto-Bliesner, B. L., and Coauthors, 2009: A comparison of PMIP2 model simulations and the MARGO proxy reconstruction for tropical sea surface temperatures at the Last Glacial Maximum. *Climate Dyn.,* **32,** 799–815.

Petit, J. R., and Coauthors, 1999: Climate and atmospheric history of the past 420,000 years from the Vostok ice core, Antarctica. *Nature,* **399,** 429–436.

Philander, S. G., and A. V. Fedorov, 2003: Role of tropics in changing the response to Milankovich forcing some three million years ago. *Paleoceanography,* **2,** 1045, doi:10.1029/2002PA000837.

Phillips, J. P., and I. M. Held, 1994: The response to orbital perturbations in an atmospheric model coupled to a slab ocean. *J. Climate,* **7,** 767–782.

Raymo, E. M., and K. Nisancioglu, 2003: The 41 kyr world: Milankovitch's other unsolved mystery. *Paleoceanography,* **18,** 1011, doi:10.1029/2002PA000791.

Rind, D., 1998: Latitudinal temperature gradients and climate change. *J. Geophys. Res.,* **103,** 5943–5971.

Shin, S.-I., Z. Liu, B. Otto-Bliesner, E. C. Brady, J. E. Kutzbach, and S. P. Harrison, 2003: A simulation of the Last Glacial Maximum climate using the NCAR-CCSM. *Climate Dyn.,* **20,** 127–151.

Soden, B. J., and I. M. Held, 2006: An assessment of climate feedbacks in coupled ocean–atmosphere models. *J. Climate,* **19,** 3354–3360.

——, A. J. Broccoli, and R. S. Hemler, 2004: On the use of cloud forcing to estimate cloud feedback. *J. Climate,* **17,** 3661–3665.

——, I. M. Held, and R. Colman, 2008: Quantifying climate feedbacks using radiative kernels. *J. Climate,* **21,** 3504–3520.

Sosdian, S., and Y. Rosenthal, 2009: Deep-sea temperature and ice volume changes across the Pliocene-Pleistocene climate transitions. *Science,* **325,** 306–310.

Stephens, G. L., 1990: On the relationship between water vapor over the oceans and sea surface temperature. *J. Climate,* **3,** 634–645.

Taylor, E. K., M. Crucifix, P. Braconnot, C. D. Hewitt, C. Doutriaux, A. J. Broccoli, J. F. B. Mitchell, and M. J. Webb, 2007: Estimating shortwave radiative forcing and response in climate models. *J. Climate,* **20,** 2530–2543.

Toggweiler, J. R., J. L. Russell, and S. R. Carson, 2006: Midlatitude westerlies, atmospheric CO_2, and climate change during the ice ages. *Paleoceanography,* **21,** PA2005, doi:10.1029/2005PA001154.

Trenberth, E. K., and J. M. Caron, 2001: Estimates of meridional atmosphere and ocean heat transports. *J. Climate,* **14,** 3433–3443.

Vimeux, F., V. Masson, J. Jouzel, M. Stievenard, and J. R. Petit, 1999: Glacial-interglacial changes in ocean surface conditions in the Southern Hemisphere. *Nature,* **398,** 410–413.

Wang, Y., S.-P. Xie, B. Wang, and H. Xu, 2005: Large-scale atmospheric forcing by southeast Pacific boundary layer clouds: A regional model study. *J. Climate,* **18,** 934–951.

Winton, M., 2000: A reformulated three-layer sea ice model. *J. Atmos. Oceanic Technol.,* **17,** 525–531.

Wittenberg, A. T., A. Rosati, N.-C. Lau, and J. J. Ploshay, 2006: GFDL's CM2 global coupled climate models. Part III: Tropical Pacific climate and ENSO. *J. Climate,* **19,** 698–722.

Wood, R., and C. S. Bretherton, 2006: On the relationship between stratiform low cloud cover and lower tropospheric stability. *J. Climate,* **19,** 6425–6432.